Max-Planck-Institut
für Mathematik
in den Naturwissenschaften
Leipzig

Least-squares hp/spectral element method for elliptic problems

(revised version: August 2009)

by

Kishore Kumar Naraparaju, and G. Naga Raju

Preprint no.: 35 2009

Least-squares hp/spectral element method for elliptic problems

N. Kishore Kumar[⋆], G. Naga Raju[†]

[⋆]Max Planck Institute for Mathematics in the Sciences,

Leipzig, Germany.

[†]Department of Mathematics and Statistics,

Indian Institute of Technology, Kanpur

India.

Abstract

The solution of elliptic boundary value problems often leads to singularities due to non-smoothness of the domains on which the problem is posed. This paper studies the performance of the nonconforming hp/spectral element method for elliptic problems on non smooth domains. This paper deals with monotone singularities of type r^α and $r^\alpha \log^\delta r$ as well as the oscillating singularities of type $r^\alpha \sin(\varepsilon \log r)$.

Key Words: Geometric mesh, least-squares solution, preconditioner, auxiliary mapping, exponential accuracy.

Mathematics Subject Classification: Primary 65M70, 65N35, 65Y05, 74B05

1 Introduction

In [1, 2] Babuska and Guo proposed an exponentially accurate method in the frame work of hp finite element method to deal the singularities in the solution. They were able to resolve the singularities which arise at the corners by using a geometric mesh. In [3] Babuska and H. S. Oh have introduced the method of auxiliary mapping (MAM). With this method exponential rates of convergence was recovered for Laplace equation with corner singularities, in the context of p version of finite element method. In [13] Lucas and Oh extended this method for Helmholtz equations.

The method of auxiliary mapping (MAM) introduced by Babuska and Oh in [3] was proven to be successful in dealing with r^α singularities. However, the effectiveness of MAM is reduced in handling $r^\alpha \sin(\epsilon \log r)$ type singularities. In [15] H. S. Oh et al., introduced the power auxiliary mapping (PAM) and the exponential auxiliary mapping (EAM) and shown that the method is highly accurate in dealing the singularities of type r^α, $r^\alpha \log^\delta r$ and $r^\alpha \sin(\epsilon \log r)$, where $0 < \alpha < 1$. They presented numerical results for various test problems and compared the results with the results obtained by the hp finite element method.

In the latest book by Pavel and Gunzburger [4] the least-squares finite element method (LS-FEM) for elliptic problems have been summarized. The standard techniques used to convert the second order elliptic equations into first order system, for example like div/curl systems shows poor rates of convergence in the presence of singularities in the solution. A weighted norm first order system least-squares (FOSLS) for problems with corner singularities have been proposed in [5, 11]. The method recovers optimal order accuracy in the weighted L^2 and H^1 norms and retains optimal L^2 convergence near the singularities. The error estimates shows only an algebraic convergence.

The elliptic problem on non-smooth domains have been examined by Pathria and Karniadakis in [16] and Karniadakis and Spencer in [8], in the framework of spectral/hp element methods. In

[19, 20] hp version of the mortar finite element method (nonconforming) have been studied. The method is optimal for both h and p version and exponential accuracy is obtained with hp version. Mathematical frame work for different discontinuous Galerkin methods for elliptic problems have been discussed in [8]. In [22] spectral/hp element methods for solving elliptic boundary value problems on polygonal domains using parallel computers were proposed. For problems with Dirichlet boundary conditions the spectral element functions were nonconforming. For problems with Neumann and mixed boundary conditions the spectral element functions have to be continuous at the vertices of the elements only and nonconforming otherwise.

In [7] P. Dutt et al. proposed an exponentially accurate nonconforming hp/spectral element method to solve general elliptic boundary value problems with mixed Neumann and Dirichlet boundary conditions on non-smooth domains. The stability and error estimates have been proved. In this paper we briefly describe the method and present the energy norm performance of elliptic boundary value problems containing the singularities of the type r^α, $r^\alpha \log^\delta r$ and $r^\alpha \sin(\epsilon \log r)$.

A geometric mesh is used in the neighbourhood of the corners and the auxiliary map of the form $z = \ln \xi$ is introduced to remove the singularities at the corners, which was first introduced by Kondratiev in [10]. In the remaining part of the domain usual Cartesian coordinate system is used.

The spectral element functions are nonconforming. The method is essentially a least-squares method and the solution can be obtained by solving the normal equations using the preconditioned conjugate gradient method (PCGM) without computing the mass and stiffness matrices [7, 9, 22]. A novel preconditioner is proposed for the method which is a block diagonal matrix, where each diagonal block corresponds to an element [6]. The condition number of the preconditioner is $O\left(\ln W\right)^2$, where W is the degree of the approximating polynomial. Let N denote the number of layers in the geometric mesh such that W is proportional to N. Then the method requires $O(W \ln W)$ iterations of the PCGM to obtain the solution to exponential accuracy.

The contents of this paper are organized as follows: In Section 2 the problem is stated and the numerical scheme is described briefly. In Section 3 computational results are provided for various test problems. The Appendix contains details of discretization of the domain and the numerical formulation in brief.

2 Numerical Scheme

The numerical method is briefly described in this Section. The complete details of the stability estimate, error estimates and numerical scheme were given in [7]. The stability estimate has been proved for strongly elliptic operator which satisfy the Babuska-Brezzi inf-sup condition on curvilinear polygons whose sides are piecewise analytic.

(i) Elliptic equation on a polygonal domain

Let Ω be a polygonal domain in $\mathbb{R}^2$ with boundary $\partial\Omega = \Gamma$ as shown in Fig.1. Let the vertices of Ω be given by $E_1, E_2, \ldots, E_p$ and the corresponding sides by the segments $\Gamma_1, \Gamma_2, \ldots, \Gamma_p$, where Γ_i joins the points E_{i-1} and E_i. Let the angle subtended at E_j be ω_j. Further, let $\Gamma = \Gamma^{[0]} \bigcup \Gamma^{[1]}$, $\Gamma^{[0]} = \bigcup_{i\in\mathcal{D}} \overline{\Gamma}_i$, $\Gamma^{[1]} = \bigcup_{i\in\mathcal{N}} \overline{\Gamma}_i$ where $\mathcal{D}$ is a subset of the set $\{i \mid i = 1, \ldots, p\}$ and $\mathcal{N} = \{i \mid i = 1, \ldots, p\} \setminus \mathcal{D}$.

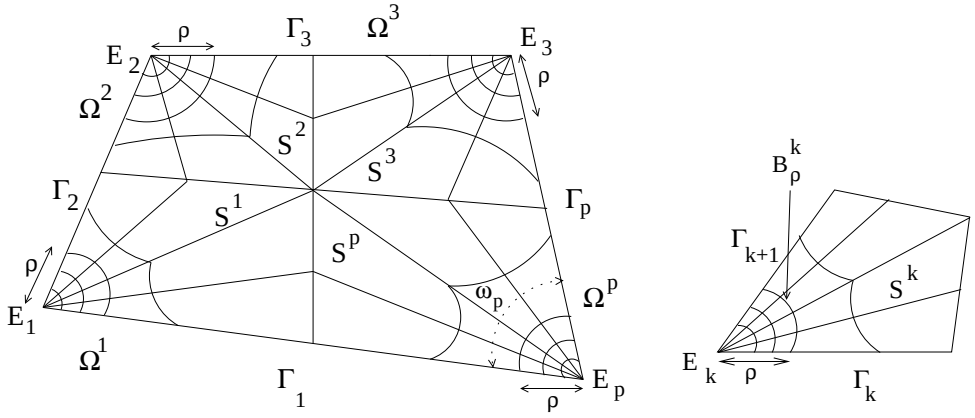

Figure 1: Polygonal Domain

Denote by $H^m(\Omega)$ the Sobolev space of functions with square integrable derivatives of integer order $\leq m$ on Ω furnished with the norm

$$\| u \|^2_{H^m(\Omega)} = \sum_{|\alpha|\leq m} \| D^\alpha u \|^2_{L^2(\Omega)} .$$

Further, let

$$\|u\|^2_{s,I} = \int_I u^2(x)dx + \int_I \int_I \frac{|u(x) - u(x')|^2}{|x - x'|^{1+2s}} dxdx'$$

denote the fractional Sobolev norm of order s, where $0 < s < 1$. Here I denotes an interval contained in $\mathbb{R}$.

Consider a two dimensional elliptic boundary value problem

$$\begin{aligned} \mathcal{L}u &= f \text{ in } \Omega, \\ u &= g^{[0]} \text{ on } \Gamma^{[0]}, \\ \left(\frac{\partial u}{\partial N}\right)_A &= g^{[1]} \text{ on } \Gamma^{[1]}. \end{aligned} \tag{2.1}$$

Here $\mathcal{L} = -\sum_{i,j=1}^{2} \frac{\partial}{\partial x_i}\left(a_{ij}(x)\frac{\partial}{\partial x_j}\right) + \sum_{i=1}^{2} b_i(x)\frac{\partial}{\partial x_i} + c(x)$ is a strongly elliptic operator which satisfy the Babuska-Brezzi inf-sup condition on Ω and the coefficients $a_{i,j}(x) = a_{j,i}(x)$, $b_i(x), c(x)$

are analytic on $\overline{\Omega}$, and $\left(\frac{\partial u}{\partial N}\right)_A$ denotes the usual conormal derivative which is defined as follows.

Let $N = (N_1, N_2)$ denote the outward normal to the curve Γ_i for $i \in \mathcal{N}$. Then

$$\left(\frac{\partial u}{\partial N}\right)_A (x) \;=\; \sum_{r,s=1}^{2} N_r a_{r,s} \frac{\partial u}{\partial x_s}\,. \tag{2.2}$$

Assume that the given data f is analytic on $\overline{\Omega}$ and $g^{[l]}$, $l = 0, 1$ is analytic on every closed arc $\overline{\Gamma}_i$ and $g^{[0]}$ is continuous on $\Gamma^{[0]}$.

(ii) Discretization and Local Transformation

Discretize the polygonal domain Ω into p non-overlapping polygonal subdomains $S^1, S^2, \ldots, S^p$, where S^k denotes a subdomain which contains the vertex E_k only. Let $S^k = \left\{\Omega^k_{i,j} : j = 1, 2, \ldots J_k,\right.$ $\left. i = 1, 2, \ldots, I_k\right\}$ be a partition of S^k, where J_k and I_k are integers (Fig. 1). I_k is bounded for all k. Let (r_k, θ_k) denote polar coordinates with center at E_k. Choose ρ so that the sector Ω^k with sides Γ_k and Γ_{k+1} bounded by the circular arc B^k_ρ centered at E_k with radius ρ, is such that $\Omega^k \subseteq S^k$. Then Ω^k can be represented as

$$\Omega^k = \left\{(x_1, x_2) \in \Omega : 0 < r_k < \rho\right\}.$$

Let $\left\{\psi^k_i\right\}_{i=1,\ldots,I_k+1}$ be an increasing sequence of points such that $\psi^k_1 = \psi^k_l$ and $\psi^k_{I_k+1} = \psi^k_u$. Let $\Delta\psi^k_i = \psi^k_{i+1} - \psi^k_i$. Choose these points so that

$$\max_k \left(\max_i \Delta\psi^k_i\right) \le \lambda \min_k \left(\min_i \Delta\psi^k_i\right)$$

for some constant λ.

Now choose a geometric mesh with N layers in Ω^k with a geometric ratio $q_k\,(0 < q_k < 1)$. Let $\sigma^k_j = \rho\,(q_k)^{N+1-j}$ for $2 \le j \le N+1$ and $\sigma^k_1 = 0$.

Let

$$\Omega^k_{i,j} = \left\{(x_1, x_2) : \sigma^k_j < r_k < \sigma^k_{j+1}, \psi^k_i < \theta_k < \psi^k_{i+1}\right\},$$

for $1 \le i \le I_k, 1 \le j \le N$.

In the remaining part of S^k, for $1 \le k \le p$, we retain the Cartesian coordinate system (x_1, x_2) i.e., in $\Omega^k_{i,j}$ for $1 \le i \le I_k, N < j \le J_k$.

Let

$$\Omega^{p+1} = \left\{\Omega^k_{i,j} : 1 \le i \le I_k, N < j \le J_k, 1 \le k \le p\right\}.$$

Relabel the elements of Ω^{p+1} and write

$$\Omega^{p+1} = \left\{\Omega^{p+1}_l, 1 \le l \le L\right\},$$

where L denotes the cardinality of Ω^{p+1}.

Now let $\tau_k = \ln r_k$ in the sector Ω^k for $1 \le k \le p$. Define $\zeta_j^k = \ln \sigma_j^k$ for $1 \le j \le N+1$. Here $\zeta_1^k = -\infty$. Define

$$\widetilde{\Omega}_{i,j}^k = \left\{(\tau_k, \theta_k) :\ \zeta_j^k < \tau_k < \zeta_{j+1}^k,\ \psi_i^k < \theta_k < \psi_{i+1}^k\right\},$$

for $1 \le i \le I_k, 1 \le j \le N$. Hence the geometric mesh $\Omega_{i,j}^k,\ 2 \le j \le N$ becomes a quasi-uniform mesh in modified polar coordinates (Fig. 2). However, $\widetilde{\Omega}_{i,1}^k$ is a semi-infinite strip.

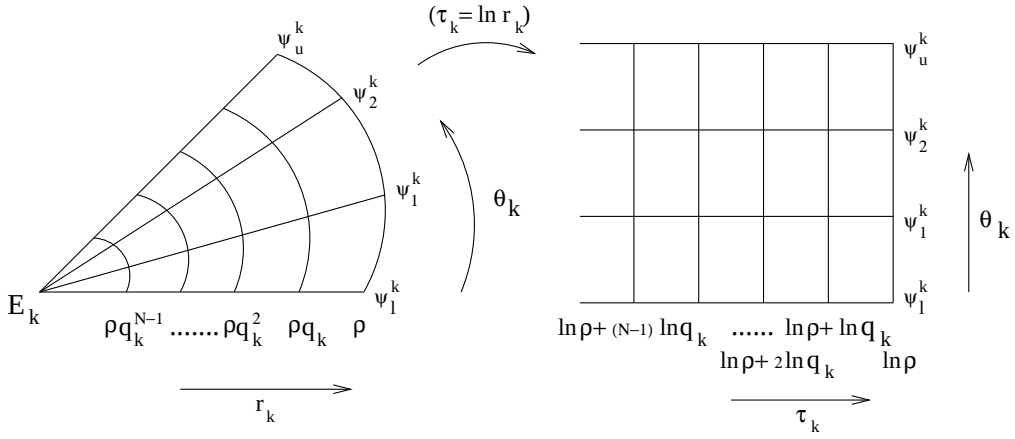

Figure 2: Quasi uniform mesh in τ_k and θ_k coordinates

(iii) Approximation

The nonconforming spectral element functions are sum of tensor products of polynomials of degree $W_j,\ 1 \le W_j \le W$ in their respective modified polar coordinates (A.1) in $\widetilde{\Omega}_{i,j}^k$ for $1 \le k \le p, 1 \le i \le I_k, 2 \le j \le N$. In the infinite sector i.e., in $\widetilde{\Omega}_{i,1}^k$, the solution is approximated by a constant which is the value of the function u at the corresponding vertex E_k. The constant value is computed by treating it as a common boundary value during the numerical computation. The quadrilateral elements of Ω^{p+1} are mapped onto the square $S = (-1,1) \times (-1,1)$ and the element function is represented as a sum of tensor product of polynomials of degree W in ξ and η, the transformed variables (A.2).

(iv) The Numerical Formulation

We seek a solution which minimizes the sum of the squares of a weighted squared norm of the residuals in the partial differential equation and the sum of the squares of the residuals in the boundary conditions in fractional Sobolev norms and enforce continuity by adding a term which measures the sum of the squares of the jump in the function and its derivatives in fractional Sobolev norms (see A.5).

The method is essentially a least-squares method and the normal equations can be solved using the preconditioned conjugate gradient method (PCGM). Let the normal equations be

$$AU = h. \tag{2.3}$$

The vector U composed of the values of the spectral element functions at Gauss-Legendre-Lobatto points is divided into two sub vectors one consisting of the values of the spectral element functions at the vertices of the domain constitute the set of common boundary values U_B (corresponding to the constant approximation in the semi-infinite strip) and the other consisting of the remaining values which we denote by U_I. Now corresponding to the decomposition of $U = \begin{bmatrix} U_I \\ U_B \end{bmatrix}$, A and h has the forms

$$A = \begin{bmatrix} A_{II} & A_{IB} \\ A_{BI} & A_{BB} \end{bmatrix} \text{ and } h = \begin{bmatrix} h_I \\ h_B \end{bmatrix}. \tag{2.4}$$

To solve the matrix equation (2.3) we use the block L-U factorization of A, viz.

$$A = \begin{bmatrix} I & 0 \\ A_{IB}^T A_{II}^{-1} & I \end{bmatrix} \begin{bmatrix} A_{II} & 0 \\ 0 & \mathbb{S} \end{bmatrix} \begin{bmatrix} I & A_{II}^{-1} A_{IB} \\ 0 & I \end{bmatrix}, \tag{2.5}$$

where the Schur Complement $\mathbb{S}$ is defined as

$$\mathbb{S} = A_{BB} - A_{IB}^T A_{II}^{-1} A_{IB}.$$

To solve the equation (2.3) based on the L-U factorization of A as given in (2.5) reduces to first solving the system of equations

$$\mathbb{S}\ U_B = \tilde{h}_B, \tag{2.6}$$

where

$$\tilde{h}_B = h_B - A_{IB}^T A_{II}^{-1} h_I. \tag{2.7}$$

Once solved for U_B using (2.6), U_I can be obtained by solving

$$A_{II} U_I = h_I - A_{IB} U_B.$$

The feasibility of such a process depends on the ability to compute $A_{IB}U_B$, $A_{II}U_I$ and $A_{BB}U_B$ for any U_I, U_B efficiently and this can always be done if AV can be computed inexpensively for any vector V. It has been shown in [22] that AV can be computed inexpensively without computing the mass and stiffness matrices.

However in addition to this it is imperative that we should be able to construct effective preconditioner for the matrix A so that the condition number of the preconditioned system is as small as possible. If this can be done then it will be possible to compute $A^{-1}V$ efficiently using the PCGM for any vector V.

It has been shown in [6] that a block diagonal matrix can be constructed as a preconditioner matrix for the matrix in the normal equations, where each diagonal block corresponds to a particular element which is mapped onto the master square S. The condition number of the preconditioned system is $O((\ln W)^2)$. Hence to compute $A^{-1}V$ to an accuracy of $O(e^{-bW})$ would require $O(W \ln W)$ iterations of the PCGM. The solution vector U is obtained to an accuracy of $O(e^{-bW})$ using $O(W \ln W)$ iterations of the PCGM.

After obtaining the nonconforming solution at the Gauss-Legendre-Lobatto points, a set of corrections are performed so that the solution is conforming and belongs to $H^1(\Omega)$. These corrections are similar to Lemma 4.57 of [18].

Then for W large enough the error estimate

$$\|u_{ex} - z\|_{1,\Omega} \leq C\, e^{-bW} \tag{2.8}$$

holds, where C and b are constants and z is the corrected solution.
The proof for this estimate follows similar to the proof of Theorem 3.1 of [23].

3 Numerical Results

To show the effectiveness of the method we considered the Laplace and the Poisson equations for which the exact solution is in one of the singular form r^α, $r^\alpha \log^\delta r$ and $r^\alpha \sin(\epsilon \log r)$. Further to check the performance of the method we have presented the results for homogeneous Helmholtz equation and for the Motz problem. Elasticity equations are also considered as an another example for showing the applicability of the method for system of equations. Taken $W_j = W$ for all j (A.1) and the number of layers N in the geometric mesh to be equal to W. The computations are carried out on a single processor. As explained in the previous Section, after obtaining the nonconforming solution a set of correction are performed so that the solution belongs to H^1. In this section we mean by Iters the total number of iterations required to compute the Schur complement matrix, solve for the common boundary value problems and finally to obtain the solution.

The relative error $\|e\|_{ER}$ is defined as $\|e\|_{ER} = \dfrac{\|e\|_E}{\|u\|_E}$, where $\|.\|_E$ denotes energy norm (H^1-norm). Since the total number of degrees of freedom (DOF) M is proportional to W^3 the relative error $\|e\|_{ER}$ in the energy norm satisfies the estimate

$$\|e\|_{ER} \leq Ce^{-bM^{1/3}}. \tag{3.1}$$

Example 1: Consider the Laplace equation on a circular domain of radius 1 as shown in Fig. 3(a) with Dirichlet boundary conditions on crack panels OA, OC and on the boundary of the circular region OAC. Let (r, θ) denote the polar coordinates with origin at the vertex $O = (0, 0)$. Let

us choose the data so that the solution u has the form of the leading singularity $r^{\frac{1}{2}}\sin(\frac{1}{2}\theta)$ at the origin. Considering the symmetry in the domain, the problem is solved on semi-circular disk as shown in Fig. 3(b). A geometric mesh is used in the neighbourhood of $O,$ with a geometric ratio $q = 0.15.$ Choose $\lambda = 1/5$ (see A.3).

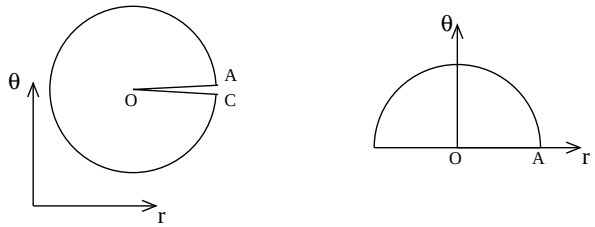

(a) (b)

Figure 3: The scheme of cracked domain

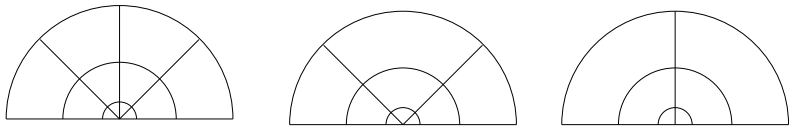

Figure 4: Geometric mesh with different mesh refinements in θ direction

In Fig. 4 the sequence of meshes for the domain Fig. 3(b) are shown, with geometric mesh refinement.

W	Mesh 1	Mesh 2	Mesh 3
2	10.0939	10.100974	10.113946
3	4.00533	4.005878	4.0100051
4	1.55574	1.556295	1.5560239
5	0.60104	0.600855	0.6000372
6	0.23338	0.233532	0.2333148
7	0.09020	0.090178	0.0900233
8	0.03500	0.034998	0.0349554
9	0.01353	0.013532	0.0135070

Table 1: Relative error in percent against W for different meshes

The values of relative error $\|e\|_{ER}$ (in percentage) are reported for different values of W in Table 1. The relative error is almost same for all the three different meshes. It is noted that the DOF is less for the discretization shown in Mesh 3 in comparison with Mesh 2 and Mesh 1. The DOF can be further reduced by using variable degree of polynomial approximation (here a uniform degree of polynomial approximation is used for computational simplicity).

W	$Iters$	M	$\|e\|_{ER}\%$	b	C
2	22	31	10.113946	0.741966	1.090843
3	40	89	4.0100051	0.745101	1.130016
4	49	191	1.5560239	0.747182	1.157822
5	66	349	0.6000372	0.747927	1.168322
6	76	575	0.2333148	0.748825	1.181549
7	87	881	0.0900233	0.749115	1.186005
8	101	1279	0.0349554	0.749944	1.199242
9	115	1781	0.0135070	0.749972	1.199703

Table 2: Values of Iterations, $M^{1/3}$, relative error (%), b and C against W

Table 2 contains the iteration count, number of degrees of freedom, the relative error in percentage and the constants b, C in (3.1) for the Mesh 3, for different values of the polynomial order W.

In Fig. 5 a graph is plotted for $log\ \|e\|_{ER}$ against $M^{1/3}$, for Mesh 3. The graph is shown to be a straight line which shows the exponential rate of convergence as it obeys exactly the error estimate (3.1).

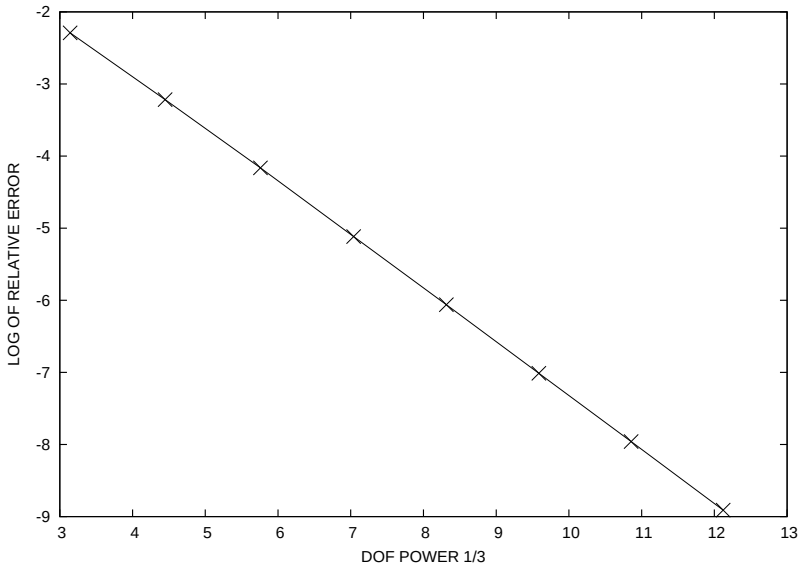

Figure 5: Log of relative error against $M^{1/3}$

Example 2: Consider the Laplace equation on a domain OAB, as shown in Fig. 6. Neumann boundary conditions are taken on sides OA, OB and Dirichlet boundary condition on the rest of the boundary. Let r and θ denote the polar coordinates with origin at the vertex O. Chosen the data such that the exact solution u has the form $r^{2/3}\cos(\frac{2}{3}\theta) + r^{4/3}\cos(\frac{4}{3}\theta)$.

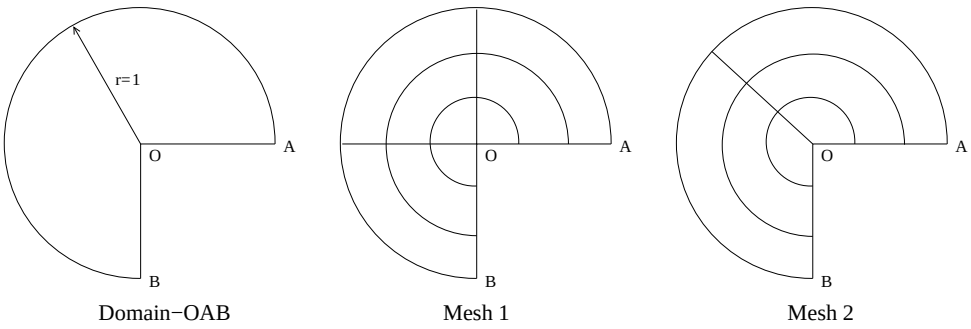

Figure 6: Sectoral domain

Mesh 1 and Mesh 2 in Fig. 6 are two different discretization of the domain with a geometric ratio $q = 0.15$. Let us choose $\lambda = 1/4$. In Table 3 the values of degrees of freedom (M) , relative error in percentage and constant values b, C for Mesh 1 and Mesh 2 are tabulated against W.

	Mesh 1		Mesh 2				
W	M	$\|e\|_{ER}\%$	M	$\|e\|_{ER}\%$	b	C	$Iters$
2	46	22.7853	31	55.4689	1.19044	10.994	20
3	133	3.1268	89	3.5228	1.14055	6.2712	38
4	286	0.5927	191	2.1518	1.14816	6.8545	52
5	523	0.1055	349	0.1151	1.05222	2.1441	71
6	862	0.0265	575	0.0494	1.07138	2.7263	87
7	1321	0.0073	881	0.0073	1.00165	1.1041	110
8	1918	0.0020	1279	0.0021	1.00501	1.1548	127
9	2671	0.0005	1781	0.0005	1.00027	1.0816	145

Table 3: Computational values for Mesh 1 and Mesh 2

Since the size of the elements is large in Mesh 2, the difference in the relative errors can be noted for smaller values of W, compared to the relative error for Mesh 1. But as W increases the error is same for both Mesh 1 and Mesh 2. The number of degrees of freedom is less for Mesh 2 and it can be further reduced by considering variable polynomial approximation.

Fig. 7 shows the graph in $M^{1/3} \times log \|e\|_{ER}$ scale. The graph is a straight line for Mesh 1 and for Mesh 2 it has some jumps initially and as W increases it becomes a straight line.

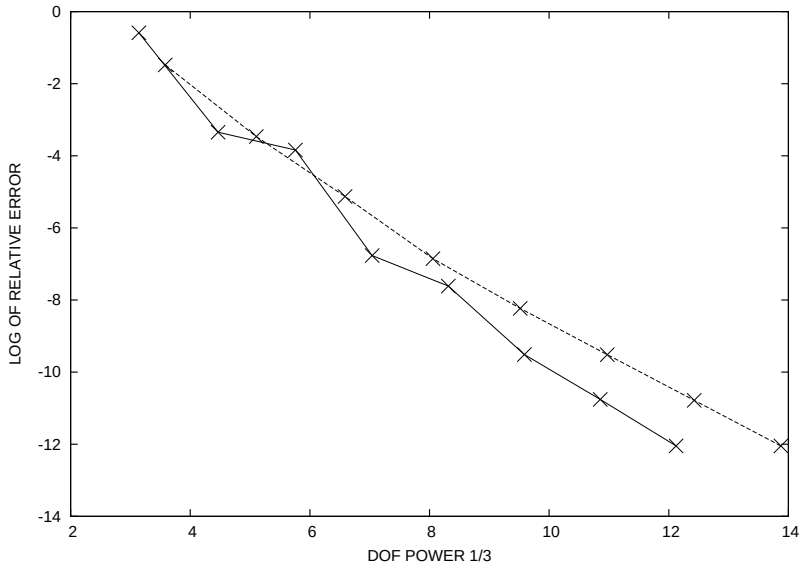

Figure 7: Log of relative error against $M^{1/3}$

Example 3: Consider a homogeneous Helmholtz equation on a domain Ω as shown in Fig. 8(a).

$$
\begin{aligned}
-\Delta u + u &= 0 \quad \text{in } \Omega, \\
\frac{\partial u}{\partial n} &= 0 \quad \text{on} \quad \Gamma_1, \\
u &= \begin{cases} \frac{\sinh(r)}{\sqrt{r}} \cos(\theta/2) & \text{on } \Gamma_2 \\ 0 & \text{on } \Gamma_3 \end{cases} .
\end{aligned}
$$

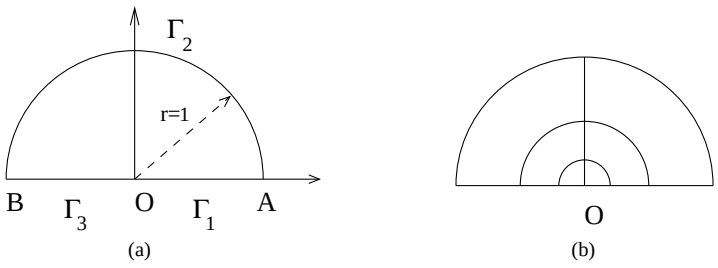

Figure 8: (a) The domain (b) Discretization

Discretization of the domain, with a geometric ratio $q = 0.15$ is shown in Fig. 8(b). The problem has a singularity at $O = (0, 0)$ and the exact solution of the problem is $\frac{\sinh(r)}{\sqrt{r}} \cos(\theta/2)$.

Let us choose $\lambda = 1/5$. In Table 4 the values of iteration count, degrees of freedom, relative error (in percentage) and constants b, C for different values of W are tabulated.

W	$Iters$	M	$\|e\|_{ER}\%$	b	C
2	18	31	16.923085	0.793474	1.9648
3	43	89	6.76869	0.790778	1.9061
4	55	191	2.037648	0.774419	1.5744
5	74	349	0.661117	0.761727	1.3500
6	89	575	0.235673	0.754788	1.2375
7	102	881	0.088490	0.751745	1.1896
8	114	1279	0.033923	0.750621	1.1719
9	127	1781	0.013098	0.750326	1.1671

Table 4: Values of Iteration count , DOF (M), the relative error (%), b and C against W

Fig. 9 shows the graph in $M^{1/3} \times log \|e\|_{ER}$ scale. The graph is a straight line and this shows the exponential rate of convergence.

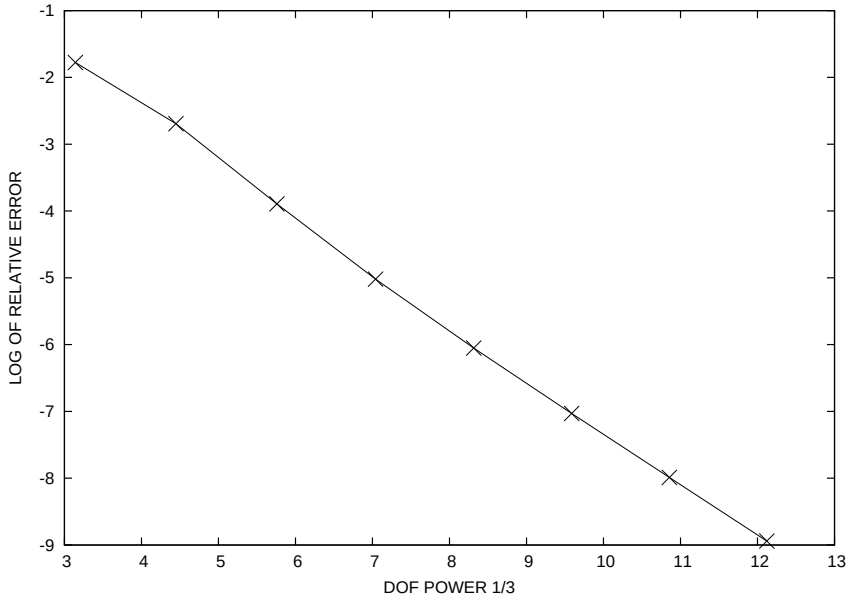

Figure 9: Log of relative error against $M^{1/3}$

Example 4: (Motz problem) Consider the Laplace's equation $-\Delta u = 0$ in a rectangular domain $\Omega_1 = \{(x, y)| -1 < x < 1, 0 < y < 1\}$ as shown in Fig. 10, satisfying the following boundary conditions

$$u|_{x<0,y=0} = 0, u|_{x=1} = 500,$$
$$u_y|_{y=1} = u_y|_{y=0,x>0} = u_x|_{x=-1} = 0.$$

This problem has been widely studied by many researchers. Rosser and Papamichael in 1975 [17] succeeded in finding the closed form solution for this problem and represented it in the fol-

lowing form

$$u = \sum_{l=0}^{P} b_l r^{l+1/2} cos(l + \frac{1}{2})\theta \tag{3.2}$$

for $P = 19$. Here (r, θ) denotes the polar coordinates.

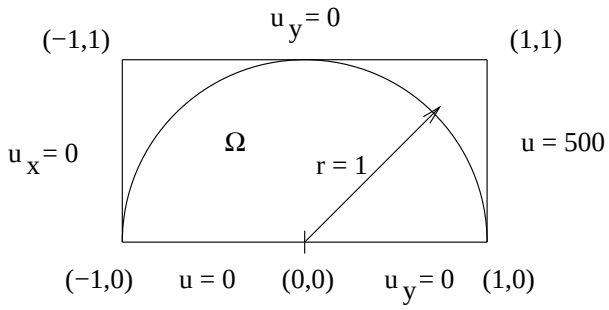

Figure 10: The domain Ω_1

For the convenience of the readers the coefficients $b_l, l = 0, 2.., 19$ are provided in the Appendix A3. More accurate solution for this problem has also been given in [12], that is for $P = 33$.

Here we have considered the Motz problem on a domain Ω which is a semi circle of radius 1 as shown in the Fig. 8(a). Chosen (3.2) as the exact solution and restricted the expansion of u on Γ_2 i.e., applied Dirichlet boundary condition on semicircular arc. Further, chosen the following conditions on the other part of the boundaries

$$u|_{\Gamma_3} = 0, \frac{\partial u}{\partial n}|_{\Gamma_1} = 0.$$

The discretization of the domain, with a geometric ratio $q = 0.15$ is as shown in Fig. 8(b). Choose $\lambda = 1/5$. In Table 5 the values of iteration count, relative error (in percentage) for different values of W are tabulated.

W	$Iters$	M	$\|e\|_{ER}\%$
2	29	31	17.4791
3	41	89	4.7940
4	60	191	1.8151
5	76	349	0.6587
6	92	575	0.2618
7	107	881	0.0969
8	119	1279	0.0375
9	135	1781	0.0145

Table 5: Values of Iteration count, relative error (%) against W.

Fig. 11 shows the graph in $M^{1/3} \times log \|e\|_{ER}$ scale which is a straight line and this indicates the exponential rate of convergence of the method.

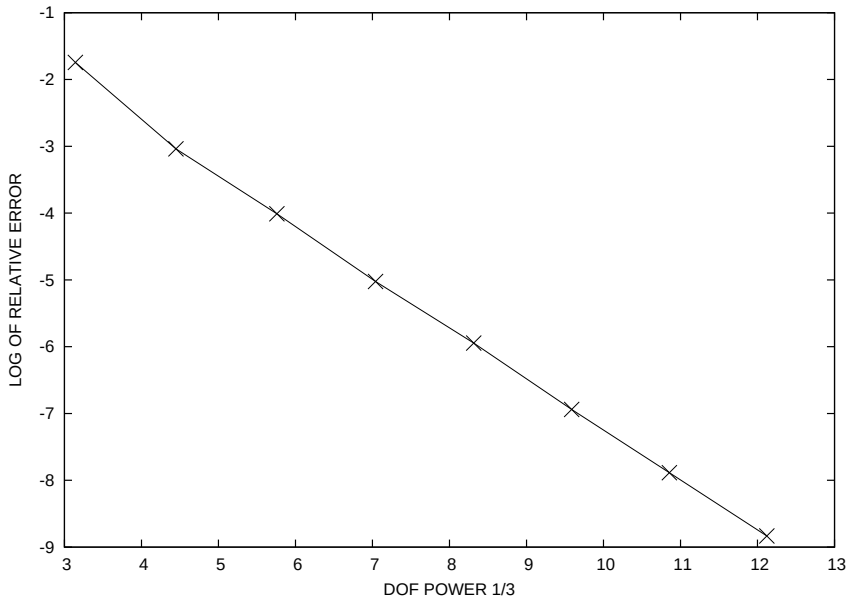

Figure 11: Log of relative error against $M^{1/3}$

Example 5: Consider the Poisson equation

$$-\triangle u = f \text{ in } \Omega = \{(r,\theta) : r \leq r_0, 0 \leq \theta \leq \pi\}.$$

In Fig. 12, the discretization of the domain Ω is shown. Chosen the data such that exact solution u is of the form $r^{0.5}\log^2 r\ \cos\theta$. Dirichlet boundary condition is imposed on $r = r_0$ and Neumann boundary condition is imposed on the remaining part of the boundary.

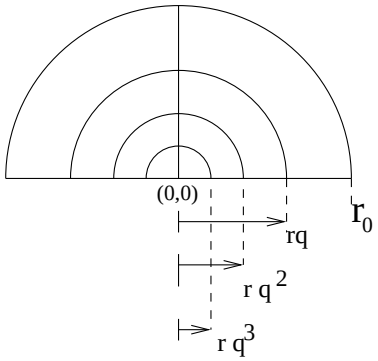

Figure 12: Discretization of the domain

As mentioned in [15], for the geometric mesh refinement the ratio $q = e^{-1.5\pi}$ gives the better results (but not optimal), here too a geometric ratio $q = e^{-1.5\pi}$ is taken for the geometric mesh and $r_0 = 2$. Auxiliary map is used over the whole domain for simplicity. Choose $\lambda = 1/5$. Table 6 contains the values of the iterations, degrees of freedom and the relative error in percentage against the degree of polynomial approximation W.

W	$Iters$	M	$\|e\|_{ER}\%$
2	25	31	37.566
3	44	89	10.212
4	64	191	3.726
5	78	349	0.765
6	94	575	0.106
7	103	881	0.012
8	115	1279	0.001
9	123	1781	0.0001

Table 6: Values of Iterations, DOF and relative error (%) against W

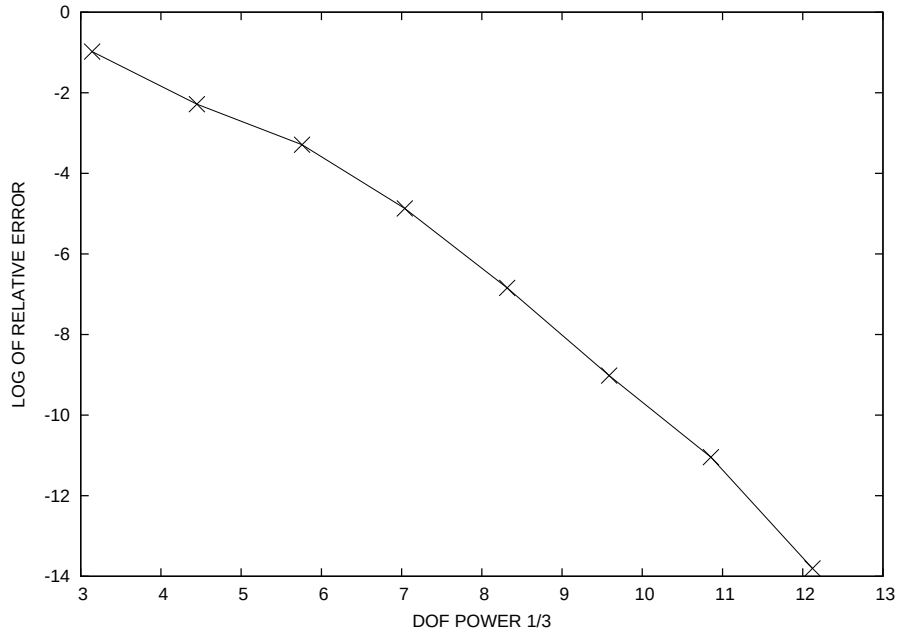

Figure 13: Log of relative error against $M^{1/3}$

Fig. 13 shows the log of relative error against degrees of freedom. Results shows that our approach gives a better results than the hp finite element method and yields the same rates of convergence as EAM comparing with the values given in [15].

Example 6: Consider the Poisson equation on the domain as shown in Fig. 12 with $r_0 = 2$. Choosing f such that the exact solution has the oscillatory singularity of the form $r^\alpha \sin(\epsilon \log r) \cos\theta$ with respect to various sizes of oscillating factor ϵ. As the oscillating factor becomes smaller, the singular function is less oscillating. Here we consider the weak singular function with $\epsilon = 0.1$ and next the highly oscillating function with $\epsilon = 3.0$.

Consider the case with $\epsilon = 0.1$ and a geometric mesh with a geometric ratio $q = e^{-1.5\pi}$. Auxiliary map is used over the whole domain for simplicity. Choose $\lambda = 1/5$.

W	$Iters$	M	$\|e\|_{ER}\%$
2	17	31	23.1583
3	38	89	4.59133
4	47	191	1.25379
5	62	349	0.19646
6	70	575	0.02104
7	86	881	0.00183
8	103	1279	0.00013
9	111	1781	0.00001

Table 7: Values of Iterations, DOF and relative error (%) against W

The computational values such as iterations, degrees of freedom and relative error in percentage are provided in Table 7 for different values of W. In Fig. 14 the log of relative error against degrees of freedom is drawn.

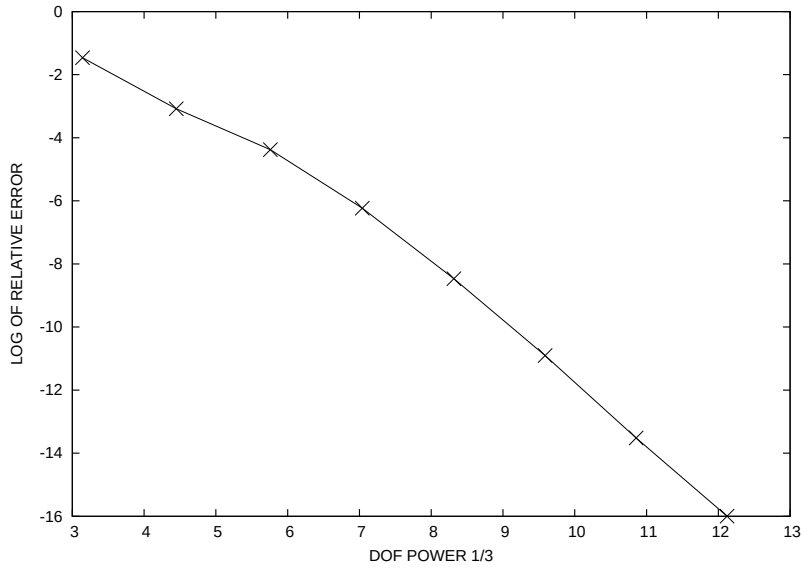

Figure 14: Log of relative error against $M^{1/3}$

Let $u = r^{0.5}\sin(\epsilon \log r)\cos\theta$ with $\epsilon = 3.0$, it is a highly oscillatory singular function. Consider $r_0 = 2$ and geometric mesh with geometric ratio $q = 0.15$. Choose $\lambda = 1/5$. The geometric ratio $q = 0.15$ gives better results among the four ratios $q = 0.15$, $q = e^{-\pi}$, $q = e^{-1.5\pi}$ and $q = e^{-2\pi}$.

Table 8 contains the values of iteration count, degrees of freedom M and relative error in percentage against W.

W	$Iters$	M	$\|e\|_{ER}\%$
2	22	31	78.166
3	36	89	54.840
4	52	191	12.04
5	64	349	6.464
6	77	575	0.68
7	85	881	0.31
8	94	1279	0.036
9	100	1781	0.010

Table 8: Values of Iterations, DOF and relative error (%) against W

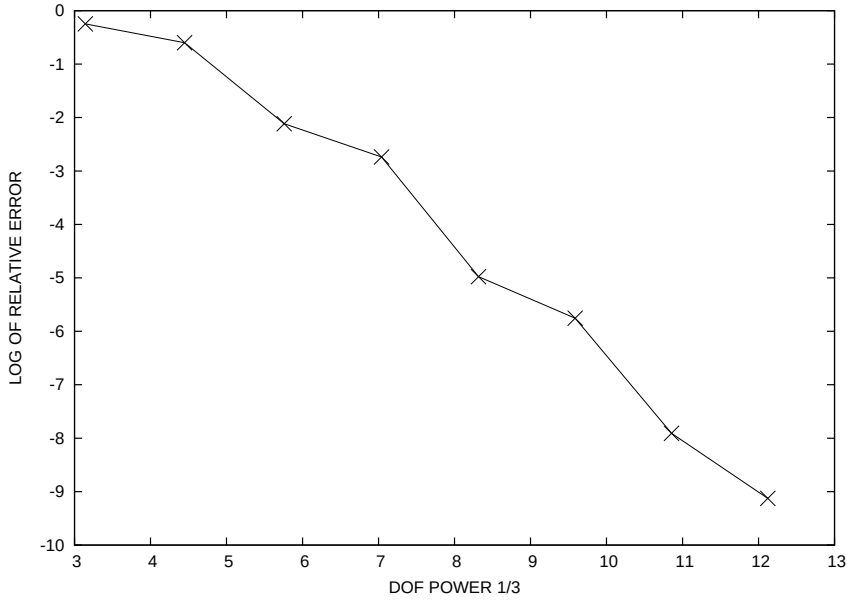

Figure 15: Log of relative error against $M^{1/3}$

Fig. 15 shows graph of the log of relative error in percentage against degrees of freedom. Results suggests that our approach gives a better results than the hp finite element method and MAM by comparing the results shown in [15].

Example 7: Let $u = (u_1, u_2)^T$ be a displacement vector. Consider the following plane strain linear elasticity problem on the domain with a re-entrant crack as shown in Fig. 16 (a) when the body forces are not present.

$$\begin{aligned} -\frac{\partial}{\partial x_1}\left(c_{11}\frac{\partial u_1}{\partial x_1} + c_{12}\frac{\partial u_2}{\partial x_2}\right) - \frac{\partial}{\partial x_2}\left[c_{66}\left(\frac{\partial u_1}{\partial x_2} + \frac{\partial u_2}{\partial x_1}\right)\right] = 0, \\ -\frac{\partial}{\partial x_1}\left[c_{66}\left(\frac{\partial u_1}{\partial x_2} + \frac{\partial u_2}{\partial x_1}\right)\right] - \frac{\partial}{\partial x_2}\left(c_{12}\frac{\partial u_1}{\partial x_1} + c_{22}\frac{\partial u_2}{\partial x_2}\right) = 0. \end{aligned} \tag{3.3}$$

Let E denote the modulus of elasticity and $\nu\,(0 < \nu < 0.5)$ denote the Poisson's ratio, then coefficients c_{11}, c_{12}, c_{22} and c_{66} are given by $c_{11} = c_{22} = \frac{E(1-\nu)}{(1+\nu)(1-2\nu)}, c_{12} = \frac{E\nu}{(1+\nu)(1-2\nu)}$, and $c_{66} = \frac{E\nu}{2(1+\nu)}$.

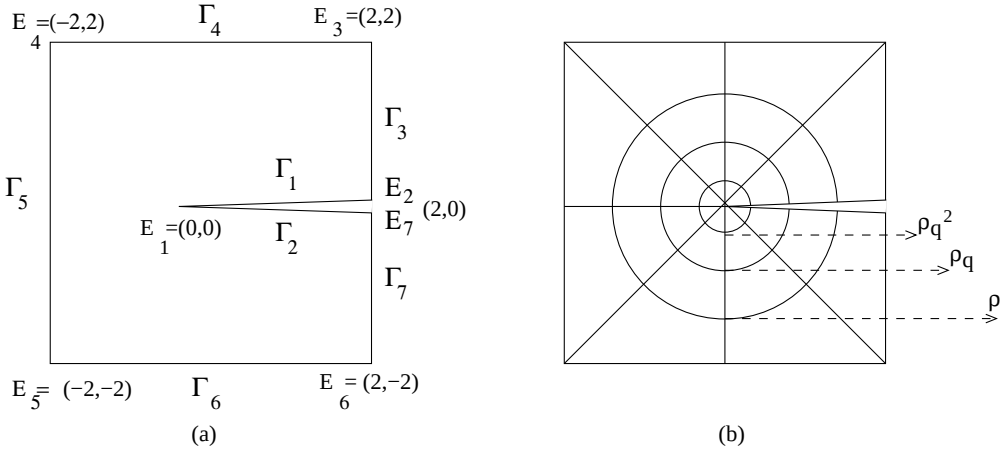

Figure 16: (a) Crack domain (b) Discretization

On the crack panels $i.e.$, on the boundary Γ_1 and Γ_2 traction boundary conditions $Tu = (T_1u, T_2u)^T$ are taken and Dirichlet boundary conditions are taken on the rest of the boundaries $\Gamma_i, i = 3...7$.

Let $n = (n_1, n_2)$ be the unit outward normal on the boundary, then the traction components T_1u and T_2u are given by

$$T_1u = \left(c_{11}\frac{\partial u_1}{\partial x_1} + c_{12}\frac{\partial u_2}{\partial x_2}\right) n_1 + c_{66}\left(\frac{\partial u_1}{\partial x_2} + \frac{\partial u_2}{\partial x_1}\right) n_2 = g_1,$$
$$T_2u = c_{66}\left(\frac{\partial u_1}{\partial x_2} + \frac{\partial u_2}{\partial x_1}\right) n_1 + \left(c_{12}\frac{\partial u_1}{\partial x_1} + c_{22}\frac{\partial u_2}{\partial x_2}\right) n_2 = g_2.$$

Let (r, θ) denote the polar coordinates with origin at E_1. The data chosen such that the solution is of the form of the leading singularity at E_1. Thus we choose the Mode 1 displacement components [21]

$$u_1 = \frac{1}{2c_{66}} r^\alpha \left[(\kappa - Q(\alpha+1))\cos\alpha\theta - \alpha\cos((\alpha-2)\theta)\right],$$
$$u_2 = \frac{1}{2c_{66}} r^\alpha \left[(\kappa + Q(\alpha+1))\sin\alpha\theta + \alpha\sin((\alpha-2)\theta)\right],$$

where $\kappa = 3 - 4\nu$, $\alpha = 0.5$ and $Q = 0.333$. Further, we choose $E = 1, \nu = 0.3$ and the geometric ratio $q = 0.15$. Let us choose $\lambda = 1/7$.

Table 9 shows the values of iteration count, relative error $\|e\|_{ER}$ in percentage against W.

W	$Iters$	M	$\|e\|_{ER}\%$
2	66	386	0.1331E+02
3	234	962	0.3720E+01
4	406	1922	0.1050E+01
5	577	3362	0.3916E+00
6	767	5378	0.1439E+00
7	1086	8066	0.5005E-01
8	1678	11522	0.1954E-01

Table 9: Values of Iterations and relative error (%) against W

In Fig. 17 a graph is plotted for $log\,\|e\|_{ER}$ against $M^{1/3}$.

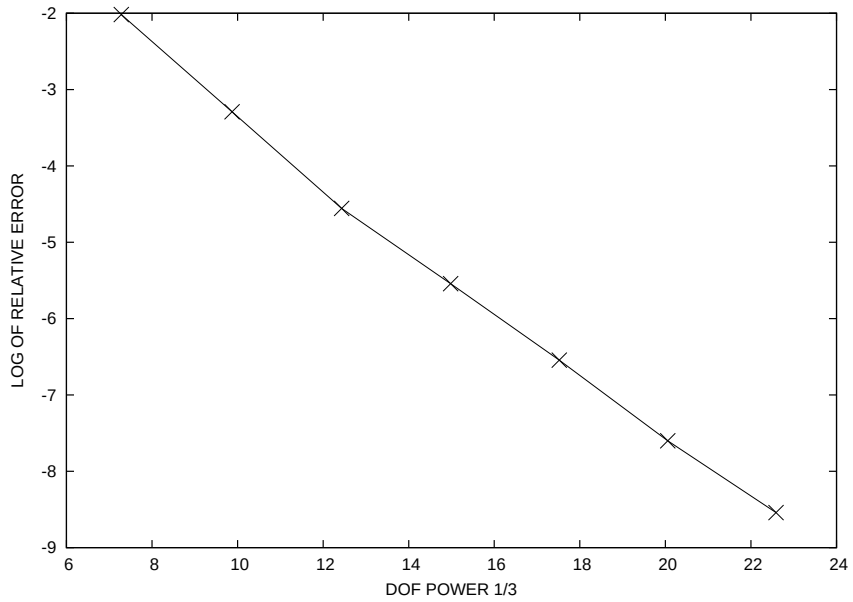

Figure 17: Log of relative error against $M^{1/3}$

Note: In example 7 the geometric mesh is used in the neighbourhood of the crack tip, shown in Fig. 16(b) as circular rings. Modified polar coordinate system is used in this region for numerical computation and away from this region usual Cartesian coordinate system is used. For all other examples the numerical computations are done by only using modified polar coordinates as the geometry of the domains in these examples supports polar coordinates easily.

Conclusions

The proposed method is exponentially accurate. The dimension of the Schur Complement matrix is small, since the cardinality of the common boundary values is small. So it is easy to construct a nearly exact approximation to the Schur Complement. The preconditioner is a block

diagonal matrix where each diagonal block corresponds to an element and it's inverse is trivial with almost optimal condition number. The algorithm for preconditioner is quite easy to implement with minimum extra effort. The residuals in the normal equation can be obtained efficiently without computing the mass and stiffness matrices. The method can also be implement on parallel computers more efficiently.

Acknowledgment

Authors gratefully acknowledge the help and guidance from Prof. P. Dutt and Prof. C.S. Upadhyay (I.I.T. Kanpur), without them this work would not have been possible.

References

[1] I. Babuska and B. Q. Guo, Regularity of the solution of elliptic problems with piecewise analytic data, Part - I, SIAM J. Math. Anal., 19 (1988), 172-203.

[2] I. Babuska and B. Q. Guo, The $h-p$ version of the finite element method on domains with curved boundaries, SIAM J. Num. Anal., 25(1988), 837-861.

[3] I. Babuska and H. S. Oh, The p version of the finite element method for domains with corners and infinite domains, Num. Meth. for Partial differential equations, 1990, 371-392.

[4] P. B. Bochev and M. D. Gunzburger, Least-squares finite element methods, Springer, 2009.

[5] Z. Cai and C. Westphal, A weighted H(div) least-squares method for second order elliptic problems, SIAM J. Num. Anal., 46, No 3(2008), 1640-1651.

[6] P. Dutt, P. Biswas and G. Naga Raju, Preconditioners for spectral element methods for elliptic and parabolic problems, J. Comput. Appl. Math., 215, No.1(2008), 152-166.

[7] P. Dutt, N. Kishore Kumar and C. S. Upadhyay, Nonconforming $h-p$ spectral element methods for elliptic problems, Proc. Indian Acad. Sci (Math. Sci.), 117(2007), 109-145.

[8] G. Karniadakis and Sherwin J. Spencer, Spectral/hp Element Methods for CFD, Oxford University Press, 1999.

[9] N. Kishore Kumar, P. Dutt and C. S. Upadyay, Nonconforming spectral/hp element methods for elliptic systems, Journal of Numer. Math., Vol. 17, No. 2 (2009), 119-142.

[10] V. A. Kondratiev, The smoothness of a solution of Dirichlet's problem for second order elliptic equations in a region with a piecewise smooth boundary, Differential' nye Uraneniya, 6(10) (1970), 1831-1843 (and Differential Equations, 6, 1392-1401).

[11] E. Lee, T. A. Manteuffel and C. R. Westphal, Weighted-Norm first order system least-squares (FOSLS) for problems with corner singularities, SIAM J. Numer. Anal. , Vol. 44, No. 5 (2006), 1974-1996.

[12] Z. C. Li, R. Mathon and P. Sermer, Boundary methods for solving elliptic problems with singularities and interfaces, SIAM J. Numer. Anal., Vol. 24, No. 3 (1987), 487-498.

[13] T. R. Lucas and H. S. Oh, The method of auxiliary mapping for the finite element solutions of elliptic problems containing singularities, Jour. Comp. Phys., 108(1993), 327-342.

[14] H. S. Oh and I. Babuska, The method of auxiliary mapping for the finite element solutions of elasticity problems containing singularities, Jour. Comp. Phys., 121(1995), 193-212.

[15] H. S. Oh, H. Kim and S. J. Lee, The numerical methods for oscillating singularities in elliptic boundary value problems, Jour. Comp. Phys., 170(2001), 742-763.

[16] D. Pathria and G.E. Karniadakis, Spectral Element Methods for Elliptic Problems in Nonsmooth Domains, Jour. Comp. Phys., 122(1995), 83-95.

[17] J. B. Rosser and N. Papamichael, MRC Technical summary report, No. 1405, University of Wisconsin, 1975.

[18] Ch. Schwab, p and $h-p$ Finite Element Methods, Clarendon Press, Oxford, 1998.

[19] P. Seshaiyer, Non-conforming hp finite element methods, Ph.D. dissertation, University of Maryland Baltimore Country, 1998.

[20] P. Seshaiyer and M. Suri, Convergence results for non-conforming hp methods: The Mortar Finite Element Method, Contemporary Mathematics, 218, 1998.

[21] B. Szabo and I. Babuska, Finite element analysis, John Wiley & Sons, 1991.

[22] S. K. Tomar, $h-p$ Spectral element method for elliptic problems on non-smooth domains using parallel computers, Computing, 78(2006), 117-143.

[23] S. K. Tomar, $h-p$ Spectral element methods for elliptic problems on non-smooth domains using parallel computers, Ph. D thesis (India: IIT Kanpur) (2001), Reprint available as Tec. Rep. no. 1631, Department of Applied Mathematics, University of Twente, The Netherlands. http://www.math.utwente.nl/publications.

A Appendix

A.1 Spectral element function

Let $u_{i,1}^k(\tau_k, \theta_k) = h_k$, a constant on $\widetilde{\Omega}_{i,1}^k$ (In the semi-infinite strip). Define the spectral element function

$$u_{i,j}^k(\tau_k, \theta_k) = \sum_{r=0}^{W_j} \sum_{s=0}^{W_j} g_{r,s}\, \tau_k^r\, \theta_k^s, \tag{A.1}$$

on $\widetilde{\Omega}_{i,j}^k$ for $1 \le i \le I_k, 2 \le j \le N, 1 \le k \le p$. Here $1 \le W_j \le W$.

Moreover there is an analytic mapping M_l^{p+1} from the master square $S = (-1,1)^2$ to Ω_l^{p+1}. Define

$$u_l^{p+1}(M_l^{p+1}(\xi, \eta)) = \sum_{r=0}^{W} \sum_{s=0}^{W} g_{r,s}\, \xi^r\, \eta^s. \tag{A.2}$$

A.2 Numerical Scheme

As described in Section 2, $\widetilde{\Omega}_{i,j}^k$ is the image of $\Omega_{i,j}^k$ in (τ_k, θ_k) coordinates. Let $\mathcal{L}^k$ be the operator defined by $\mathcal{L}^k u = r_k^2\, \mathcal{L} u$. Let $y_1 = \tau_k$ and $y_2 = \theta_k$ then

$$\tilde{\mathcal{L}}^k u = -\sum_{i,j=1}^{2} \frac{\partial}{\partial y_i}(\tilde{a}_{i,j}^k \frac{\partial u}{\partial y_j}) + \sum_{i=1}^{2} \tilde{b}_i^k \frac{\partial u}{\partial y_i} + \tilde{c}^k u.$$

Let

$$O^k = \begin{bmatrix} \cos\theta_k & -\sin\theta_k \\ \sin\theta_k & \cos\theta_k \end{bmatrix} \quad \text{and} \quad \tilde{A}^k = \begin{bmatrix} \tilde{a}_{1,1}^k & \tilde{a}_{1,2}^k \\ \tilde{a}_{2,1}^k & \tilde{a}_{2,2}^k \end{bmatrix}.$$

Then $\tilde{A}^k = (O^k)^T A O^k$, where A is the matrix $(A)_{r,s} = a_{r,s}$.

Next, let the vertex $E_k = \left(x_1^k, x_2^k\right)$ and

$$F_{i,j}^k(\tau_k, \theta_k) = e^{2\tau_k} f\left(x_1^k + e^{\tau_k}\cos\theta_k, x_2^k + e^{\tau_k}\sin\theta_k\right)$$

in $\tilde{\Omega}_{i,j}^k$ for $1 \le k \le p$, $2 \le j \le N$, $1 \le i \le I_k$ (since $\mathcal{L}^k u = r_k^2\, f$).

Let $\gamma_s \subseteq \Gamma^{[1]} \cap \partial\Omega^k$ for $1 \le k \le p$, and $\tilde{\gamma}_s$ denote the image of γ_s in (τ_k, θ_k) coordinates. Now the unit normal n at a point $\tilde{P}$ on $\tilde{\gamma}_s$ can be written as $n = (n_1, n_2)$. Then

$$\left(\frac{\partial u^k}{\partial n}\right)_{\tilde{A}^k} = \sum_{i,j=1}^{2} n_i\, \tilde{a}_{i,j}^k \frac{\partial u^k}{\partial y_j}.$$

Consider the boundary conditions $u = g_k$ on $\Gamma_k \cap \partial\Omega^k$ for $k \in \mathcal{D}$, and $\left(\frac{\partial u}{\partial N}\right)_A = g_k$ on $\Gamma_k \cap \partial\Omega^k$

for $k \in \mathcal{N}$. Let

$$l_1^k(\tau_k) = \begin{cases} u = g_k(x_1^k + e^{\tau_k} cos(\psi_l^k)\,,\, x_2^k + e^{\tau_k} sin(\psi_l^k)), & \text{for } k \in \mathcal{D}, \\ \left(\frac{\partial u}{\partial n}\right)_{\tilde{A}^k} = e^{\tau_k}\, g_k(x_1^k + e^{\tau_k} cos(\psi_l^k)\,,\, x_2^k + e^{\tau_k} sin(\psi_l^k)), & \text{for } k \in \mathcal{N}. \end{cases}$$

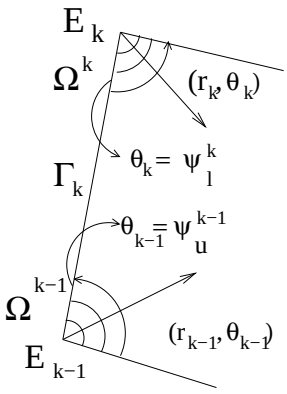

Figure 18: Edge Γ_k common to Ω^{k-1} and Ω^k

Consider the boundary condition $u = g_k$ for $k \in \mathcal{D}$, and $\left(\frac{\partial u}{\partial N}\right)_A = g_k$ for $k \in \mathcal{N}$ on $\Gamma_k \cap \partial\Omega^{k-1}$. Define

$$l_2^k(\tau_{k-1}) = \begin{cases} u = g_k(x_1^{k-1} + e^{\tau_{k-1}} cos(\psi_u^{k-1})\,,\, x_2^{k-1} + e^{\tau_{k-1}} sin(\psi_u^{k-1})), & \text{for } k \in \mathcal{D}, \\ \left(\frac{\partial u}{\partial n}\right)_{\tilde{A}^k} = e^{\tau_{k-1}} g_k(x_1^{k-1} + e^{\tau_{k-1}} cos(\psi_u^{k-1})\,,\, x_2^{k-1} + e^{\tau_{k-1}} sin(\psi_u^{k-1})) & \text{for } k \in \mathcal{N}. \end{cases}$$

Now we consider the elements in Ω_l^{p+1}. In Ω_l^{p+1} for $1 \le l \le L$,

$$\int_{\Omega_l^{p+1}} \left|\mathcal{L}u_l^{p+1}\right|^2 dx_1 dx_2 = \int_S \left|\mathcal{L}u_l^{p+1}\right| J_l^{p+1}\, d\xi d\eta.$$

Here J_l^{p+1} is the Jacobian of the mapping M_l^{p+1} from S to Ω_l^{p+1}. Define $\mathcal{L}_l^{p+1} = \sqrt{J_l^{p+1}}\,\mathcal{L}$.

Let $f_l^{p+1}(\xi,\eta) = f(M_l^{p+1}(\xi,\eta))$ for $1 \le l \le L$ and define $F_l^{p+1}(\xi,\eta) = f_l^{p+1}(\xi,\eta)\sqrt{J_l^{p+1}(\xi,\eta)}$.

By γ_s we shall denote a side common to the elements Ω_m^{p+1} and Ω_n^{p+1}. It may be assumed that γ_s is the image of $\eta = -1$ under the mapping M_m^{p+1} which maps S to Ω_m^{p+1} and also the image of $\eta = 1$ under the mapping M_n^{p+1} which maps S to Ω_n^{p+1}. By the chain rule

$$\begin{aligned} (u_m^{p+1})_{x_1} &= (u_m^{p+1})_\xi\ \xi_{x_1} + (u_m^{p+1})_\eta\ \eta_{x_1}, \text{ and} \\ (u_m^{p+1})_{x_2} &= (u_m^{p+1})_\xi\ \xi_{x_2} + (u_m^{p+1})_\eta\ \eta_{x_2}. \end{aligned}$$

Then

$$\begin{aligned} \left\|[u^{p+1}]\right\|_{0,\gamma_s}^2 &= \left\|u_m^{p+1}(\xi,-1) - u_n^{p+1}(\xi,1)\right\|_{0,I}^2, \\ \left\|[(u_{x_i}^{p+1})]\right\|_{1/2,\gamma_s}^2 &= \left\|(u_m^{p+1})_{x_i}(\xi,-1) - (u_n^{p+1})_{x_i}(\xi,1)\right\|_{1/2,I}^2,\ i = 1,2. \end{aligned}$$

Here I is the interval $(-1,1)$.

Next, let $\gamma_s \subseteq \Gamma^{[0]} \cap \partial\Omega^{p+1}$ and let γ_s be the image of $\eta = -1$ under the mapping M_m^{p+1} which maps S to Ω_m^{p+1}. Then

$$\left\|u^{p+1}\right\|_{0,\gamma_s}^2 + \left\|\left(\frac{\partial u^{p+1}}{\partial T}\right)\right\|_{1/2,\gamma_s}^2 = \left\|u_m^{p+1}(\xi,-1)\right\|_{0,I}^2 + \left\|\left(\frac{\partial u_m^{p+1}}{\partial T}\right)(\xi,-1)\right\|_{1/2,I}^2.$$

In the same way if $\gamma_s \subseteq \Gamma^{[1]} \cap \partial\Omega^{p+1}$, $\left\|\left(\frac{\partial u^{p+1}}{\partial N}\right)_A\right\|_{1/2,\gamma_s}^2$ can be defined.

Let $\Gamma_k \bigcap \partial\Omega_m^{p+1} = C_m^k$ be the image of the mapping M_m^{p+1} of S onto Ω_m^{p+1} corresponding to the side $\eta = -1$, and $o_m^k(\eta) = g_k\left(M_m^{p+1}(\xi,-1)\right)$, where $-1 \le \xi \le 1$.

Let $\gamma_s \subseteq \bar{\Omega}^k$ and $d(E_k,\gamma_s) = \inf_{x\in\gamma_s}\{\text{distance}(E_k,x)\}$. Choose $\lambda_k < \alpha_k$ where α_k is defined as in [7]. Let $\mathcal{F}_u = \left\{\left\{u_{i,j}^k(\tau_k,\theta_k)\right\}_{i,j,k}, \left\{u_l^{p+1}(\xi,\eta)\right\}_l\right\} \in \Pi^{N,W}$, the space of spectral element functions. Define $a_k = u(E_k)$.

Define the functional

$$\begin{aligned}
\mathfrak{r}_{vertices}^{N,W}(\mathcal{F}_u) &= \sum_{k=1}^{p}\sum_{j=2}^{N}\sum_{i=1}^{I_k}(\rho\mu_k^{N+1-j})^{-2\lambda_k}\left\|(\widetilde{\mathcal{L}}^k)u_{i,j}^k(\tau_k,\theta_k) - F_{i,j}^k(\tau_k,\theta_k)\right\|_{0,\tilde{\Omega}_{i,j}^k}^2 \\
&+ \sum_{k=1}^{p}\sum_{\substack{\gamma_s\subseteq\Omega^k\cup B_\rho^k,\\ \mu(\tilde{\gamma_s})<\infty}} d(E_k,\gamma_s)^{-2\lambda_k}\left(\left\|[u^k]\right\|_{0,\tilde{\gamma_s}}^2 + \left\|[(u_{\tau_k}^k)]\right\|_{1/2,\tilde{\gamma_s}}^2 + \left\|[(u_{\theta_k}^k)]\right\|_{1/2,\tilde{\gamma_s}}^2\right) \\
&+ \sum_{m\in\mathcal{D}}\sum_{k=m-1}^{m}\sum_{\substack{\gamma_s\subseteq\partial\Omega^k\cap\Gamma_m,\\ \mu(\tilde{\gamma_s})<\infty}} d(E_k,\gamma_s)^{-2\lambda_k}\left(\left\|(u^k-h_k)-(l_{m-k+1}^m-a_k)\right\|_{0,\tilde{\gamma_s}}^2\right. \\
&\quad \left.+ \left\|u_{\tau_k}^k - (l_{m-k+1}^m)_{\tau_k}\right\|_{1/2,\tilde{\gamma_s}}^2\right) + \sum_{m\in\mathcal{D}}\sum_{k=m-1}^{m}(h_k-a_k)^2 \\
&+ \sum_{m\in\mathcal{N}}\sum_{k=m-1}^{m}\sum_{\substack{\gamma_s\subseteq\partial\Omega^k\cap\Gamma_m,\\ \mu(\tilde{\gamma_s})<\infty}} d(E_k,\gamma_s)^{-2\lambda_k}\left\|\left(\frac{\partial u^k}{\partial n}\right)_{\tilde{A}^k} - l_{m-k+1}^m\right\|_{1/2,\tilde{\gamma_s}}^2. \qquad \text{(A.3)}
\end{aligned}$$

In the above $\mu(\tilde{\gamma_s})$ denotes the measure of $\tilde{\gamma_s}$.

Define

$$\begin{aligned}
\mathfrak{r}_{interior}^{N,W}(\mathcal{F}_u) &= \sum_{l=1}^{L}\left\|(\mathcal{L}_l^{p+1})u_l^{p+1}(\xi,\eta) - F_l^{p+1}(\xi,\eta)\right\|_{0,S}^2 \\
&+ \sum_{\gamma_s\subseteq\Omega^{p+1}}\left(\left\|[u^{p+1}]\right\|_{0,\gamma_s}^2 + \left\|[(u_{x_1}^{p+1})]\right\|_{1/2,\gamma_s}^2 + \left\|[(u_{x_2}^{p+1})]\right\|_{1/2,\gamma_s}^2\right) \\
&+ \sum_{l\in\mathcal{D}}\sum_{\gamma_s\subseteq\partial\Omega^{p+1}\cap\Gamma_l}\left(\left\|u^{p+1}-o^l\right\|_{0,\gamma_s}^2 + \left\|\left(\frac{\partial u^{p+1}}{\partial T}\right) - \left(\frac{\partial o^l}{\partial T}\right)\right\|_{1/2,\gamma_s}^2\right) \\
&+ \sum_{l\in\mathcal{N}}\sum_{\gamma_s\subseteq\partial\Omega^{p+1}\cap\Gamma_l}\left\|\left(\frac{\partial u^{p+1}}{\partial N}\right)_A - o^l\right\|_{1/2,\gamma_s}^2. \qquad \text{(A.4)}
\end{aligned}$$

Let

$$\mathfrak{r}^{N,W}(\mathcal{F}_u) = \mathfrak{r}^{N,W}_{vertices}(\mathcal{F}_u) + \mathfrak{r}^{N,W}_{interior}(\mathcal{F}_u). \tag{A.5}$$

We choose as our approximate solution the unique $\mathcal{F}_z \in \Pi^{N,W}$, the space of spectral element functions, which minimizes the functional $\mathfrak{r}^{N,W}(\mathcal{F}_u)$ over all $\mathcal{F}_u$.

The numerical scheme presented is based on the stability estimate, Theorem 3.2 of [7]. The stability estimate in addition with the trace theorems for Sobolev spaces ensures the norm equivalence of residual norms and the solution norm.

A.3 The coefficients in the solution of the Motz problem

l	b_l	l	b_l
0	401.1624537452	10	0.0073023017
1	87.6559201951	11	-0.0031841139
2	17.2379150794	12	0.0012206461
3	-8.0712152597	13	0.0005309655
4	1.4402727170	14	0.0002715122
5	0.3310548859	15	-0.0001200463
6	0.2754373445	16	0.0000505400
7	-0.0869329945	17	0.000023167
8	0.0336048784	18	0.000011535
9	0.0153843745	19	-0.000005295

Table 10: Coefficients b_l